AIAA JOURNAL
Vol. 38, No. 5, May 2000

Results for a Two-Component Doppler Global Velocimeter

Steve Naylor* and John Kuhlman†
West Virginia University, Morgantown, West Virginia 26506-6106

A two-component Doppler global velocimeter (DGV) system is described, and velocity measurements obtained to quantify its accuracy are presented. Molecular iodine vapor cells are used as frequency discriminating filters to determine the Doppler shift of laser light that is scattered off of seed particles in a flow, from which velocity is determined. Results are presented for velocity distributions over the surface of a rotating wheel, a fully developed pipe flow, and a freejet. For the rotating wheel DGV results, rms noise levels display standard deviations of ± 1 m/s, whereas total velocity range errors are between ± 1 and 2 m/s out of 59 m/s. The rms error is dominated by residual errors in the flat-field correction, and the 8-bit camera resolution, whereas velocity range errors are largely influenced by iodine cell calibration accuracy. Measurements for fully developed turbulent pipe flow and axisymmetric jet flow show good agreement with pitot-static probe data. A random velocity offset error due to iodine cell side arm temperature variations of about 4–5 m/s has been found to be the dominant error source in the present DGV system. A reference tab has been used to record the zero velocity signals in the pipe and jet flows.

Introduction

THE accuracy of Doppler global velocimetry (DGV), a nonintrusive, planar imaging, Doppler-based velocimetry technique, is studied in the current work. DGV uses an iodine vapor cell absorption line filter (ALF) to determine Doppler shift, and hence velocity, of small seed particles in a flowfield, as these particles pass through a two-dimensional sheet of laser light. The same portion of the light sheet is viewed through a beam splitter by a pair of video cameras, with the ALF placed in the optical path of one of the cameras. Laser wavelength and ALF absorption band are matched such that the range of flow velocities of interest yields Doppler shifted frequencies that lie in the linear portion of the absorption band of the ALF. As a result, the ratio of the light intensities seen by the two detectors at a point in the flow yields a signal proportional to the particle velocity. Use of conventional charged-coupled device (CCD) cameras to view the light sheet yields velocity data at an effective resolution of at least 100 pixels by 100 lines, at framing rates of up to 30 frames/s, at a typical velocity accuracy of on the order of about 5% of full scale. This reduced accuracy relative to conventional laser velocimetry (LV) is primarily due to camera noise and pixel registration errors, as well as laser speckle noise for systems using pulsed Nd:YAG lasers.[1,2]

A two-component point Doppler velocimeter (PDV) system has been previously developed by Kuhlman et al.[3] A two-component, planar imaging DGV system using CCD cameras has also recently been developed, as initially described by Naylor and Kuhlman.[4] The accuracy limits of both systems are being systematically explored, through a series of measurements in relatively simple flows. A rotating wheel is also being used as a velocity standard. The present paper describes the two-component DGV system and related software and presents a series of velocity measurements for a rotating wheel, a fully developed pipe flow, and a freejet, to assess the accuracy of the DGV system for mean velocity measurements.

Literature Summary

Several different nonintrusive whole-field velocimetry techniques are under development that provide velocity data in a plane, which can, thus, greatly reduce the time required to map out a complex flowfield and can also lead to enhanced insight into flow physics. Of these techniques, particle image velocimetry (PIV) has been the most fully developed.[5] Scalar imaging velocimetry shows promise for determination of three-dimensional velocity data in large Schmidt number liquid flows.[6] Another nonintrusive technique under development by Miles is the RELIEF technique,[7] which appears to be limited to two velocity components in a plane, similar to PIV.

DGV, the aforementioned concept for acquiring nonintrusive real-time velocity measurements in a planar region, was originally demonstrated by Komine et al.[8] This technique uses a pair of video cameras and an iodine vapor cell for each velocity component to measure the Doppler frequency shift of the light scattered off minute seed particles in a flow as they pass through a planar sheet of laser light. A group at the NASA Langley Research Center led by Meyers[9] is developing DGV into an accurate instrument. NASA Langley Research Center has also funded work by Meyers and Komine.[10]

Others are also developing concepts similar to DGV; for example, Miles et al.[11] have developed a filtered Rayleigh scattering technique that allows nonintrusive velocity measurements without requiring any seeding. An optically thick ALF is used to filter out all signals but the Doppler shifted frequencies due to molecular Rayleigh scattering. Accuracy of this technique in supersonic flows has been documented by Forkey et al.[12] to be comparable to that of DGV on a percentage basis.

Hoffenberg and Sullivan[13] have measured jet velocity using a point filtered particle scattering technique. Accuracy of mean and turbulence quantities was comparable to LV data near the centerline at the exit of a low-speed axisymmetric jet. However, large errors in mean and rms velocities were found near the edges of the jet, probably due to uneven seeding and low signal-to-noise ratio. Similar PDV studies have been conducted by Morrison et al.,[14] Roehle and Schodl,[15] and Kuhlman et al.[3]

More recently, McKenzie,[1,16] Smith and Northam,[2] Smith,[17] Irani,[18] and Irani and Miller,[19] Elliott et al.,[20,21] Clancy et al.,[22] Mosedale et al.,[23] Reinath,[24] Beutner and Baust,[25] Beutner et al.,[26] and Ainsworth and Thorpe[27] have also developed DGV systems. Meyers[28] describes recent improvements to his DGV systems. Several systems have used a single video camera to record both the reference and signal images for each velocity component; this split-image technique reduces resolution by a factor of two, but also reduces system cost and complexity. The data by McKenzie[16] for point measurements on a rotating wheel display an absolute accuracy on the order of ±1–2 m/s. McKenzie's more recent planar DGV results of the velocity of the same rotating wheel displayed a lower level of accuracy (±2–5 m/s).[1] Two-component PDV results by Kuhlman et al.[3] for a rotating wheel displayed an accuracy on the order of ±0.5–1 m/s.

Received 24 December 1998; presented as Paper 99-0268 at the AIAA 37th Aerospace Sciences Meeting, Reno, NV, 11–14 January 1999; revision received 4 October 1999; accepted for publication 12 October 1999.

*Graduate Student, Mechanical and Aerospace Engineering Department. Student Member AIAA.

†Professor, Mechanical and Aerospace Engineering Department. Associate Fellow AIAA.

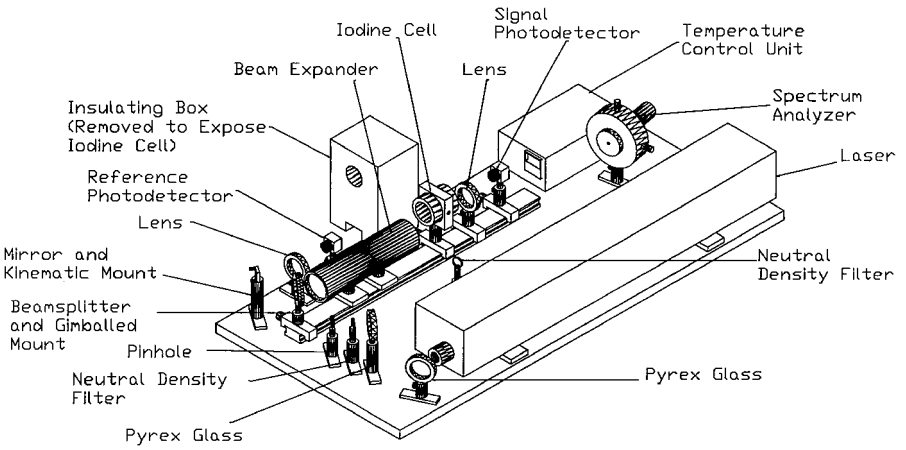

Fig. 1 Schematic of reference system.

Thus, it is clear that, in a very short time, DGV has demonstrated capability for making nonintrusive mean flow velocity vector measurements in a plane, in a variety of complex flowfields of practical significance. Although current DGV systems lack the accuracy or resolution of conventional LV systems or PIV, DGV has proven to be a flexible whole-field velocimetry technique.

Following the notation of McKenzie,[16] the basic equation relating the Doppler shift frequency to the resolved velocity component is given by

$$\delta v = [(\boldsymbol{o} - \boldsymbol{i}) \cdot \boldsymbol{V}]/\lambda \tag{1}$$

where δv is the Doppler frequency shift, $\boldsymbol{V}$ is the velocity vector, λ is the incident laser frequency, and $\boldsymbol{o}$ and $\boldsymbol{i}$ are the observer and laser propagation directions, respectively. Thus, the resolved velocity component is in the direction of the difference of unit vectors $\boldsymbol{o}$ and $\boldsymbol{i}$. Viewing the light sheet from three different directions enables determination of the three-dimensional velocity field in a plane.

Apparatus

The present DGV system has been patterned after the basic DGV configuration originally developed by Meyers et al.,[9] in an effort to document the accuracy that is attainable with such DGV systems. System hardware and software (see next section) have been described in more detail by Naylor and Kuhlman[4] and in the dissertation by Naylor.[29‡] A reference iodine cell has been used to compensate for changes (due to laser frequency drift) in the voltage ratios for the iodine cells that view the flow and receive the Doppler shifted scattered light. This reference iodine cell system is shown in Fig. 1. The present iodine cells are 2 in. in diameter, with a 2-in. optical path length, and contain both solid- and vapor-phase iodine. Neutral density filters and a beam expander are used to ensure that neither the iodine cell nor either photodiode is saturated by the reference beam. The laser used is a Coherent Innova 305 argon ion laser fitted with an etalon for single-frequency operation. A laser spectrum analyzer has been used to monitor laser mode shape and to detect the occurrence of mode hops.

Achieving adequate temperature stability of the side arms of the iodine cells has been found to be an essential requirement for accurate operation of a DGV system.[9] The present cell temperature control system comprises a pair of electrical band heaters that heat a hollow bushing made from oxygen-free copper, which surrounds the iodine cell except for the two optical windows and the side arm. The side arm has been thermally heat sunk by a copper wire that is bonded to the tip of the side arm and then bolted to the optical breadboard on which the DGV system is mounted. This lowers the temperature of the side arm and ensures that any solid-phase iodine collects there instead of on the cell ends. The Omega proportional integral-derivative (PID) temperature controller has been adjusted to maintain a constant cell side arm (cold finger) temperature by heating the cell body, where the copper sheath surrounding the iodine cell typically operates at temperatures nominally 10°C above the side arm temperature. Cells have been operated at stem temperatures of 45°C, resulting in line center transmission of between 5 and 10%.

Data acquisition software has been developed in Visual Basic 4.0 to allow monitoring and data acquisition of the cell temperatures for the reference cell and each of the cells used in the two DGV components. Long-term drift in iodine cell stem temperature has been measured to be on the order of ±0.1–0.2°C once the cells have warmed up to steady operating temperature, and short-term stem temperature fluctuations have an rms of 0.1°C or less.[29] An 8-channel, 16-bit, simultaneous-sample-and-hold IOTech analog-to-digital (A/D) board is used for digital data acquisition of the photodetector output voltages for the reference system. The rms noise level for this board is ±0.3 mV on a 10-V scale. Windows-based data acquisition software has been developed (again using Visual Basic) for this board.

A rotating wheel apparatus has been used to determine the accuracy of the two-component DGV system. The wheel is a 12-in.-diam, anodized circular aluminum disk that has been painted white, mounted to a variable speed dc motor. This wheel has a maximum linear velocity of approximately ±29 m/s.

A fully developed turbulent pipe flow apparatus has been developed using 1.5-in.-diam pipe with a length-to-diameter ratio of 60. This flow is driven by a variable-speed blower and has been run at an exit velocity of nominally 42 m/s, corresponding to a Reynolds number of 1×10^5. Flow seeding for DGV measurements is provided by a commercial ROSCO fog machine, which feeds a large plenum, to damp out pulsations in smoke output. This has led to better uniformity in the signal levels from image to image for the pipe and jet flow data. Also, the amount of smoke produced has been reduced by placing a diode in series with the motor that drives the fog fluid pump. This has improved the quality of data, most likely by reducing the effects of secondary scattering.

A computer-controlled, three-axis traversing system has been developed, as described in the thesis by Ramanath,[30] for use in positioning the flow facilities with respect to the fixed DGV system, so that velocity contours may be mapped out in a series of planar cuts through a flow. Accuracy of a single traverse move has been found to be better than 0.001 in. for typical moves on the order of a few inches.[30]

Hitachi KP-M1 CCD 8-bit cameras and a Matrox Genesis frame grabber are being used for the two-component DGV system. The frame grabber has four inputs, each leading to 8-bit digitizers. All four cameras are read simultaneously by using horizontal and vertical synchronization signals from the Genesis board. The continuous data acquisition rate, writing to the hard drive, for the two-component DGV system is approximately two sets of four frames/s, whereas short bursts of data (10 frames total from each camera) may be acquired at 30 frames/s by using the onboard memory of the Genesis board.

Figure 2 shows one of two DGV channels. Attached to the front of the cameras are Nikon 35–135 mm zoom lenses mounted on C-mount adapters. Zoom lenses were selected instead of fixed focal

‡Available in pdf format at http://www.wvu.edu/~thesis/ (select "Search WVU ETDS" and "Browse") [cited 5 April 2000].

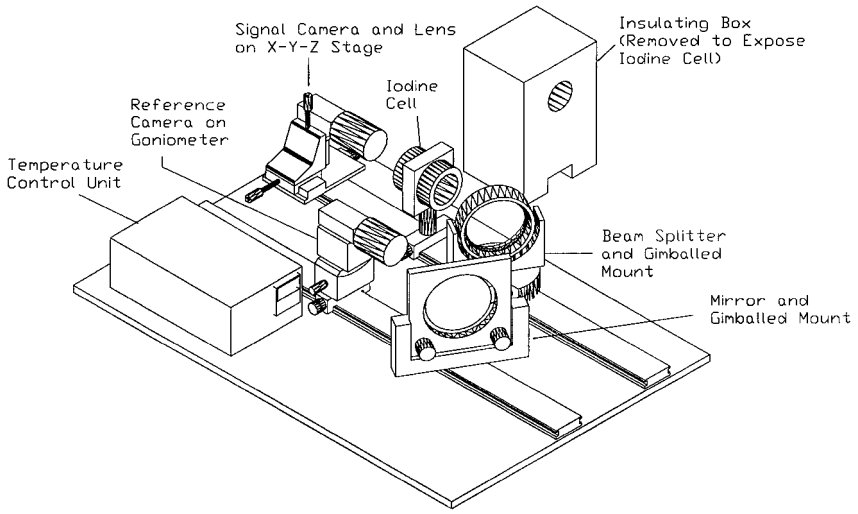

Fig. 2 Schematic of a DGV measuring component.

length lenses because of their versatility in imaging different sized areas over a wide range of distances. The penalty paid for this flexibility is an increased f-number for a given focal length relative to a fixed focal length lens. This both decreases the amount of incoming light and somewhat increases the noise due to laser speckle.[1,2] Polarizing filters have been placed in front of the beam splitters to minimize effects due to polarization sensitivity of the beam splitters.[18]

Data Acquisition and Image Processing

Introduction

The software written for both image processing and the operation of the frame grabber is a mixture of C and Visual Basic; see the dissertation by Naylor[29] or the paper by Naylor and Kuhlman[4] for a more complete description. Visual Basic provides the front end for all grabbing and processing dynamic linking libraries (DLLs), which have been written in C.

Iodine Cell Calibration

Calibration of the iodine cells has been accomplished by scanning the mode structure of the argon ion laser, by mechanically altering the tilt of the etalon through about 10–20 mode hops, over a 20–30-s period. Spacing between modes of 120 MHz, based on the laser cavity length, establishes the relative frequency axis. Because only a relatively narrow frequency range can be scanned in this fashion (about 40 modes), it has not been possible to determine which iodine absorption line has been used by matching the experimental transmission profile with the iodine absorption model of Forkey.[12] It is generally noted that the signal-to-reference ratio for each iodine cell varies somewhat between mode hops. Because discrete changes in laser power accompany mode hops, their occurrence has been detected by a sudden jump in reference photodiode voltage. This continuous scan mode hop calibration technique offers better accuracy than an earlier technique, where individual ratio values were measured after each mode hop of the laser.[31] This is because the cell temperatures cannot change significantly over the 20–30-s time period required to perform a scan. Also, the effects due to variability of where one stops the mechanical screw adjust on the etalon tilt screw are minimized by this technique.

James[31] also obtained significant further improvement in calibration accuracy by averaging several of these individual continuous scan mode hop calibrations together. This improved calibration consists of several (from 7 to 10) continuous mode hop calibration data sets for each cell. A single cell calibration data file is formed by sliding all mode hop calibrations along the relative frequency axis, to overlay them on one arbitrarily selected calibration scan of the set using linear interpolation. This is necessary because of laser drift between individual mode hop calibrations, where the ratio value for the nth mode hop for any one cell will change, especially when the room temperature varies significantly. After the calibration data is shifted, a best-fit curve is found, using a nonlinear least-squares

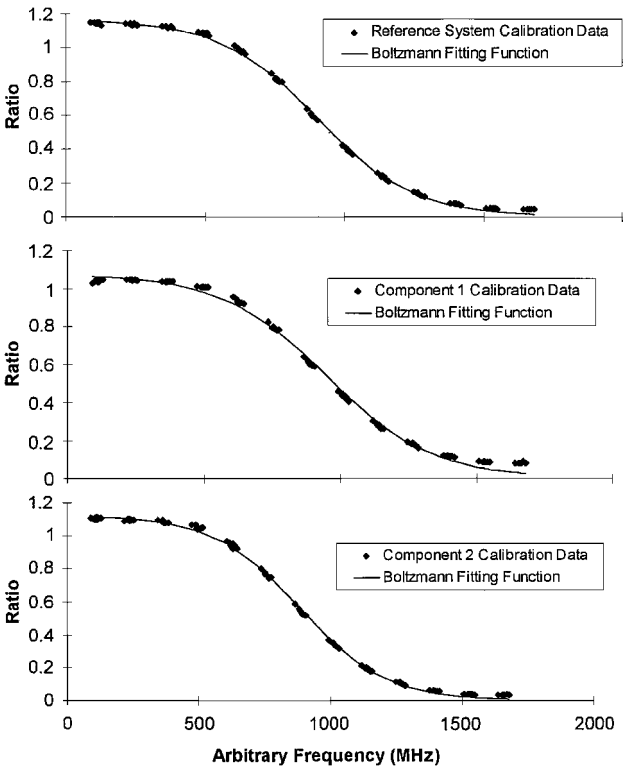

Fig. 3 Calibration data and curve fits for reference, component 1, and component 2 iodine cells.

technique, to determine a relative frequency given a measured ratio using a form of a Boltzmann fitting function given as

$$y = (A_1 - A_2) \Big/ \left(1 + \exp\left(\frac{x - x_0}{D_x} + A_2\right)\right) \tag{2}$$

where A_1 and A_2 are the top and bottom boundary ratio levels, respectively, x_0 is a horizontal frequency shift, and D_x is a horizontal stretching coefficient. Figure 3 shows a sample of this curve fit with calibration data for each of the three iodine cells. This function has been used rather than a theoretically based function partly because it has been difficult to obtain mode hop data that cover both sides of the absorption line. There appears to be room for improvement in the curve-fitting function shape near the top and bottom of the curves; the present velocity results have been acquired near the middle of these curves. The standard deviation of the Boltzmann curve fit from the data averages 0.012 MHz for the reference and measurement calibrations over the portions of the curves used in the

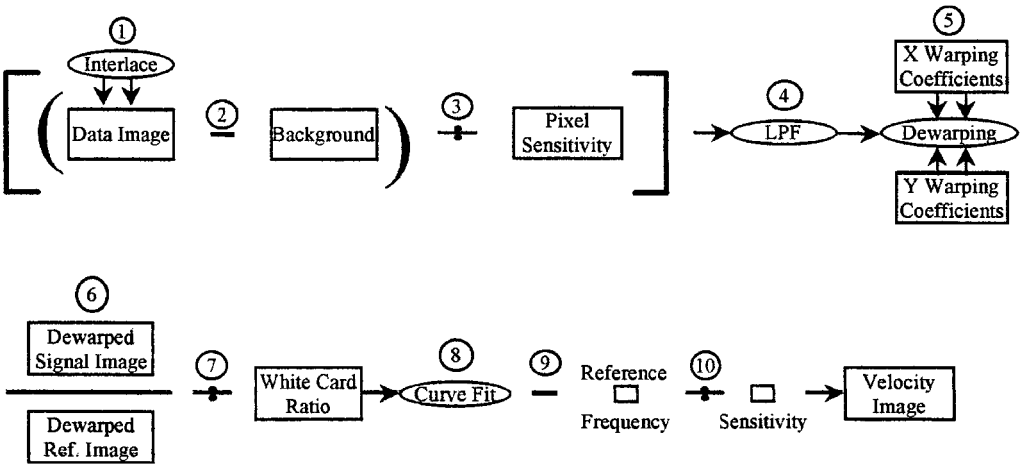

Fig. 4 Block diagram of image processing steps (steps 1–5 performed on each image; steps 6–10 combine signal and reference images).

measurements. For the DGV measurement systems, cells are calibrated using the video cameras and camera lenses, set up exactly as for the DGV data collection. Scattered light from seed particles in the flow, moving at very low velocity (~1 m/s), is used for this calibration. As a result, no normalization of the calibration curves has been performed (Fig. 3). The average gray level within a user-defined area for each of these calibration images is calculated and recorded before further data shifting and curve fitting is performed.

Image Processing Software

A block diagram of the data reduction process is shown in Fig. 4; this software has been described by Naylor.[29] Most of the steps shown closely follow the comprehensive image processing methods developed at NASA Langley Research Center by Meyers.[32,33] All DGV data taken consist of fields because the cameras are interlaced. Thus, the first step image processing step is to form a complete frame, filling in the missing odd lines with the average of the neighboring lines of data. Besides the cell calibrations, several additional images need to be taken before each data run while the system remains undisturbed. The first of these additional images is the background image. The background image is an average of several frames of the data area without laser illumination, which is subtracted from all data images subsequently taken in an effort to remove CCD dark current noise and background illumination.

The next averaged image is one of a rectangular reference grid of small dots placed in the plane of the light sheet that is key to the spatial corrections needed for accurate alignment of the signal and reference camera images. This dot card image provides reference points with which images are mapped to the rectangular grid and overlaid.

An averaged image of a laser-illuminated white card (flat-field correction) is also recorded, with the iodine cells in place. Laser light is used, rather than broadband or white light, and the laser is tuned such that the frequency does not fall in an iodine absorption line during this acquisition.[1] The signal and reference images for the flat-field correction image are processed in the same fashion as the data images through calculation of the signal-to-reference ratio (step 6 of Fig. 4). Then, the flat-field ratio image for each channel is normalized with respect to the corresponding image average ratio value. The resulting matrix of floating point numbers should, ideally, be equal to 1.0, but spatial imperfections in the imaging system (lenses, beam splitters, mirrors, and cell ends) cause variations in the ratio that are typically as much as ±5%. Data images with ratios thus determined are then divided by the white card (flat-field) matrix to correct for these imperfections.[33] Naylor[29] has clearly shown the need for this correction in his analysis of rotating wheel results.

The flat-field correction does not account for the slight variations in the sensitivity of individual pixels across the CCD array. To force all pixels in an array to have the same sensitivity, two average images are taken with all lenses removed and the array exposed to two different light levels. Individual pixel sensitivities (or slopes), which, ideally, should be equal to 1.0, are calculated at each pixel by

$$\text{slope}_{x,y} = \frac{P1_{x,y} - P2_{x,y}}{\text{av1} - \text{av2}} \tag{3}$$

where $P1_{x,y}$ is the gray level value at the x, y pixel location in the first image, and $P2_{x,y}$ is the pixel value at the same location in the second image. Here av1 and av2 are the average gray level values for the first and second images, respectively. The correction is applied by dividing the data image from each camera by the corresponding array of pixel slopes.[32] Naylor and Kuhlman[4] have shown an example of X and Y cuts through the center of a flat-field image from one of the cameras before and after the pixel sensitivity correction has been applied. Also, the pixel sensitivity array for each camera displays a distinct, organized spatial pattern when displayed as a false color image of the uncorrected pixel slope arrays. Typical signal-to-noise ratios (SNRs) for the X and Y cuts before the correction are 280 and 160, respectively, based on the rms and the full 256 gray level range. After the correction, the SNR is increased to 320, with no discernible spatial pattern remaining in colorized corrected images.

The next step in the algorithm is to low-pass filter the image resulting from the preceding steps. A convolution is performed between a flat 5 × 5 kernel and the image, in effect, blurring it. Low-pass filtering reduces the effects of both the CCD readout noise, as well as any laser speckle noise.[1] The spatial resolution of the camera–lens combination, determined by the response to a step change from black to white, has been found to be approximately 3–5 pixels wide, so that a 5 × 5 kernel actually causes minimal loss of meaningful spatial variations in velocity.[29]

The need for mapping of images onto the rectangular grid (dewarping) is most obvious when trying to overlay velocity images from different DGV channels to resolve orthogonal velocity components. Resolution of those components necessitates measuring velocity from different viewing directions, resulting in perspective distortions. However, even though both signal and reference cameras within a DGV component system are viewing the same area through a beam splitter, dewarping is also needed for these images to correct for imperfect pixel-to-pixel alignment.[32] The dewarping process begins with the acquisition of a dot card image for each camera, as described earlier, which provides an array of discrete reference points with which to overlay the images. Each dot card image is masked by thresholding the result of a standard edge-finding (Sobel) filter. The masked image is then analyzed to find the dot center (centroid) locations. The numbers of rows and columns of dots visible in the distorted image are counted, and the grid coordinates are calculated in such a way as to fill the entire dewarped image with that number of equally spaced points. Next, the X and Y coordinates of the dewarped image that correspond to locations in the warped (dot card) image are found by finding the ratio of the distances to the nearest dots and equating the ratios in both the warped and dewarped

images.[34] These numbers represent noninteger pixel locations in the warped image that are used in bilinear interpolation performed on each pixel to yield the target gray level value in the dewarped image.

Accuracy of the dewarping routines has been tested by recording two sets of dot card images, the second of which was translated horizontally and vertically through a distance equal to one-half of the dot spacing. The first set of dot card images was processed as described to compute the dewarping coefficients, which were then applied to the computed dot card centroid coordinates for the second set of images. If the dewarping process were without error, then the horizontal X distances and the vertical Y distances that each dot centroid moved in the dewarped images would be the same. For this data set, the computed rms of the X and Y distances that each centroid moved was approximately 0.1 pixel. Also, the rms of the difference between computed distances for corresponding dot centroids in the signal and reference camera images for the two DGV channels was 0.2–0.3 pixels for the rotating wheel data and 0.3–0.4 pixels for the pipe and jet data, taken with a higher lens magnification.[29] This compares favorably with similar results by McKenzie,[1] where a value of 0.3 pixels has been given. Clancy et al.[22] have demonstrated that this subpixel accuracy is required for good accuracy of the DGV method.

The dewarped signal and reference images for each component are then divided, producing a ratio image containing values that are proportional to velocity. The pixel ratio is passed through the inverted curve fit of the appropriate cell calibration data, resulting in a relative frequency value. The pixel locations that have either signal or reference camera signal levels that are either saturated or below a threshold grayscale level of five are marked and recorded. The reference frequency is then subtracted from both relative frequency arrays of the two components, to compensate for laser drift. The pixels marked as having low or high gray level values are omitted from all subsequent averaging and statistical calculations, and the marked pixels are assigned a delta frequency value of zero for image display purposes.

At this point there exist two frequency images that are used in Eq. (1) to produce two velocity images by dividing the frequency images by the corresponding component sensitivity to produce velocity images. These velocity images are then averaged, on an individual pixel basis, where data for pixel values marked as below the threshold are omitted from the averaging. This is necessary for the pipe and jet velocity data because of the drop off in signal near the edges of the flows where there is a reduction in the amount of flow seeding.

Results

Introduction

The results presented in this section are from a two-component DGV setup represented schematically for the wheel velocity data runs in Fig. 5. Results have been obtained for a rotating wheel, fully developed turbulent pipe flow, and axisymmetric jet flow. The laser beam exits the laser and enters the X–Y scanner head, which, for wheel velocity data, is stationary and simply acts as a turning mirror. This X–Y scanner has been used to generate a laser light sheet that has been used to illuminate cross-sectional cuts of the pipe and jet flows.

For the wheel velocity data, the beam is steered through a 9-mm focal length biconvex lens, creating a cone of laser light that is projected onto the surface of the wheel. Imperfections on the surface of the lens create circular interference fringes visible on the surface of the wheel. Two layers of opaque plastic film placed in the expanded beam as optical diffusers remove any visible intensity variations.[1] The DGV sensing components have been placed at relatively shallow angles with respect to the incident laser beam to maximize their sensitivity to the direction of motion of the wheel. However, sensitivity to velocity normal to the plane of the wheel is reduced. For the angles shown, components 1 and 2 have sensitivities of 2.19 and 3.07 MHz/(m/s), respectively. Furthermore, component 2 is aligned so that it measures 82% of the wheel velocity, compared to 40% for component 1.

Wheel Velocity Results

Four sets of rotating wheel data have been acquired, two sets at a wheel setting of maximum speed clockwise and two sets at maximum speed counterclockwise. Each set was taken on the same day and reduced using the same cell calibrations (Fig. 3), acquired just prior to the velocity data. Typical two-component DGV velocity results will be presented, taken from the work of Naylor.[29] Figure 6 shows an average grayscale image of the computed tangential velocity, and Fig. 7 shows the corresponding computed normal velocity image. For the motor speed setting used, and the diameter of the wheel, the calculated full velocity range (top to bottom) is 58.7 m/s. Plots of the DGV velocity along horizontal X and vertical Y cuts through the tangential velocity image of Fig. 6 are shown in Fig. 8. These results are the processed average of 30 images. An offset on the order of 5 m/s in the DGV measurements has been subtracted from both cuts. The cause of this zero velocity offset is believed to be random, uncorrelated drift in the side arm temperatures of the reference and measurement iodine cells; similar zero offsets were observed in the PDV results of Kuhlman et al.[3] The rms deviation of the tangential velocity in Fig. 6 from the known solid body wheel rotation varies from 1.2 to 1.8 m/s for X and Y cuts, with an average rms error of 1.5 m/s, for a series of four runs.[29] RMS errors in the normal velocity (Fig. 7) are higher, ranging from 3.0 to 3.9 m/s, with an average error of 3.4 m/s for the four runs. The measured tangential velocity range has been found by placing a least-squares linear fit through a vertical cut taken down the center of the velocity image and subtracting the two endpoint values of the fit. Percent error has been calculated with respect to the correct range of 58.7 m/s for all runs. The tangential velocity range errors are between 5 and 8% for

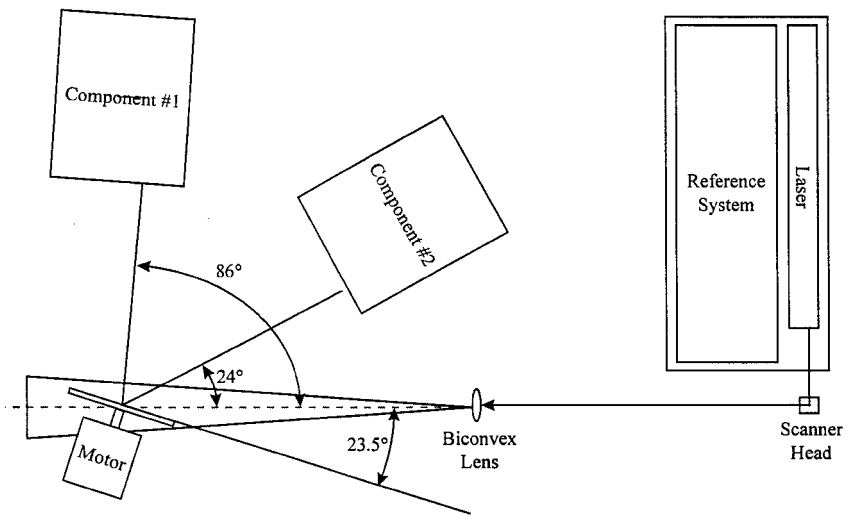

Fig. 5 Top-view schematic of system geometry for rotating wheel experiment.

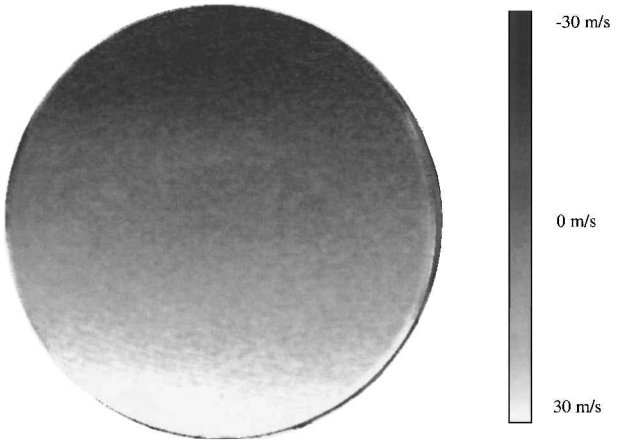

Fig. 6 Grayscale two-component DGV tangential average velocity image of rotating wheel.

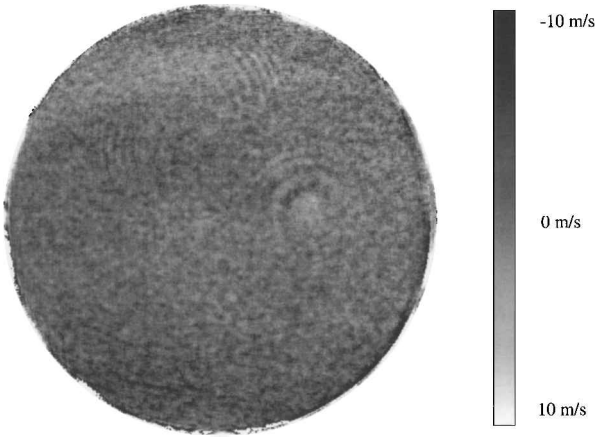

Fig. 7 Grayscale two-component DGV normal average velocity image of rotating wheel.

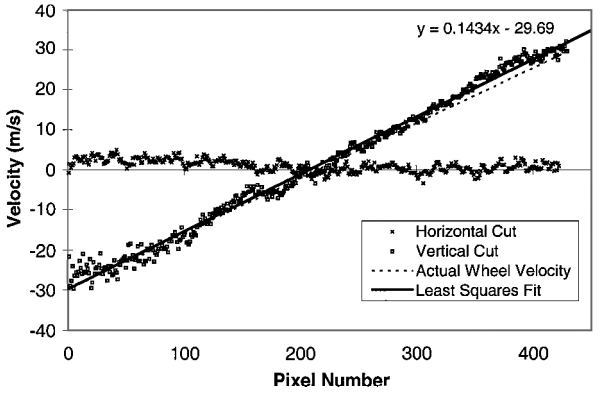

Fig. 8 Horizontal and vertical cuts through average of 30 DGV velocity images of rotating wheel: tangential velocity data of Fig. 6.

the four runs.[29] The dissertation by Naylor[29] presents false color images of these DGV wheel velocity results. Note that wiggles with a peak-to-peak magnitude on the order of 4 m/s are visible in both the X and Y cuts shown in Fig. 8. These are believed to be due to imperfections in the flat-field or white card corrections. Without the flat-field correction these errors are on the order of 15 m/s (Ref. 29).

Naylor[29] has shown these same rotating wheel data, reduced as two independent DGV systems, where the tangential velocity has been computed by dividing the measured velocities along each channel's sensitivity direction by the cosine of the angle between the sensitivity direction and the known tangential direction for the wheel. DGV component 2, which is more sensitive to the wheel velocity, yields rms errors of 0.9–1.3 m/s, and velocity range errors of

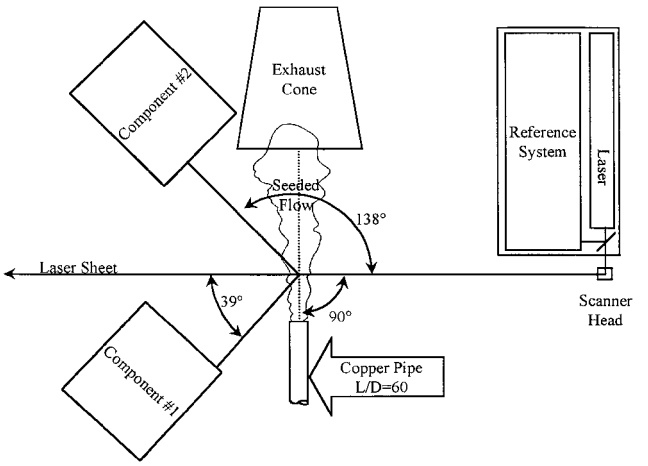

Fig. 9 Top-view schematic of system geometry for turbulent pipe flow and jet experiments.

0.9–2.6% of the known velocity range of 58.7 m/s. Component 1 displays larger rms errors (2.2–3.3 m/s) and larger tangential velocity range errors (12–19% of 58.7 m/s).

The observed iodine cell side arm rms temperature fluctuation of ±0.1°C has been found to result in a predicted rms frequency error of 1.75 MHz, based on the theoretical iodine absorption model of Forkey.[12] Assuming these rms temperature fluctuations for the reference and measurement cells to be uncorrelated results in a predicted error in measured Doppler shift of 7 MHz, based on two standard deviations (95% confidence level). This frequency error would then result in a velocity error of between 2 m/s (for backscatter viewing directions) and 10 m/s (for forward scatter viewing directions), showing this to be the source of the dominant error in the present system. These predicted velocity errors due to cell side arm temperature variations are consistent with the observed mean velocity offset errors in the present work. This suggests that the present iodine cells should be replaced with vapor-limited cells in the future.[20–23]

Inconsistencies in the cell calibrations also result in bias errors, which are partly responsible for the errors in the velocity range. Analysis of the repeatability of the cell calibrations performed on different days produces a maximum error of ~1.4 m/s or 2.4%, based on the maximum ratio range recorded for the data images for component 2 (Ref. 29). This error magnitude is consistent with the observed errors in velocity range.

Pipe and Jet Velocity Results

The configuration geometry for the pipe and jet flow measurements is shown in Fig. 9. The x–y scanner has been used to generate light sheet illumination in crossflow planes, where fully developed turbulent pipe flow data have been obtained by illuminating the flow at the pipe exit (approximately 0.2 in. downstream of the exit, to avoid direct illumination of the pipe surface). A large cone has been connected to a blower to exhaust the seeded flow from the laboratory. Both DGV components have been configured in forward scatter to obtain similar signal strengths from both channels. This has allowed operation of the system with all camera lenses essentially wide open (ƒ3.5–4), so that the amount of smoke in the flow could be adjusted to obtain gray levels in the center of the flow of 200–220 for both channels out of the full-scale range of 255. Note, however, that this geometry made it impossible to obtain DGV velocity measurements from component 1 at the pipe exit because the line of sight from component 1 to the pipe exit is physically blocked by the copper pipe (Fig. 9). The speed of the blower that fed the pipe flow apparatus has been adjusted to balance the jet flow rate with the maximum exhaust blower flow rate. This yielded a centerline exit velocity of 42 m/s based on pitot-static probe data, corresponding to an exit Reynolds number of 1×10^5 based on the pipe diameter.

For the setup shown in Fig. 9, Naylor has presented false color images of velocity results for both fully developed turbulent pipe flow and axisymmetric jet flow.[29] Examples of X and Y cuts through these DGV velocity images are shown in Figs. 10 and 11. These

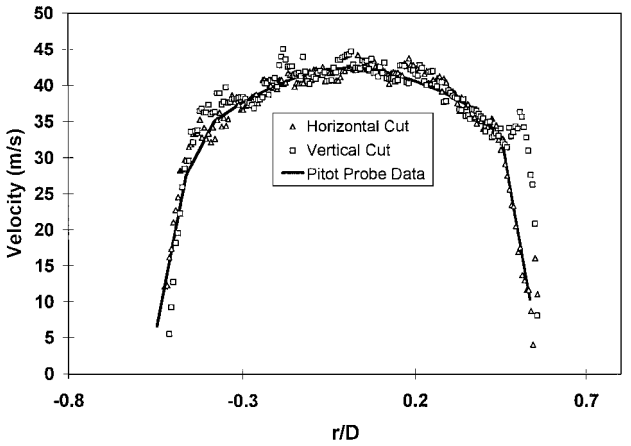

Fig. 10 Comparison of DGV pipe flow velocity measurements and pitot-static probe data: horizontal and vertical cuts at pipe exit, component 2.

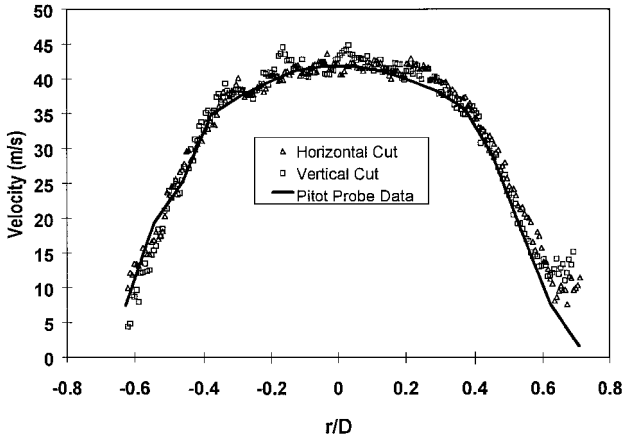

Fig. 11 Comparison of DGV jet flow velocity measurements and pitot-static probe data: horizontal and vertical cuts, component 2 at $x/D = 1$.

mean velocity images are the average of 30 individual images, acquired over a 10–15 s time period. For these data, a small white paper tab has been illuminated with unshifted laser light via a fiber optic cable and lens,[29] and light scattered from this tab has been recorded in all DGV data images as a zero velocity reference signal, following procedures developed by McKenzie.[1] Data in Fig. 10 have been obtained at the pipe exit from DGV component 2. The measured DGV velocity data in the sensitivity direction have been divided by the cosine of the angle between this sensitivity direction and the known mean velocity direction along the pipe axis. These data have been compared with pitot-static probe data. DGV results show good symmetry and generally agree to within an offset of 2–4 m/s with the pitot-static probe data. As in the DGV rotating wheel results, a pattern of wiggles in the velocity data having a total range of about 4 m/s is seen for both cuts; these are again due to imperfections in the flat-field correction image. Figure 11 shows X and Y cuts through an average DGV image for the jet flow at a distance of 1 diameter from the exit, and a grayscale image of these jet velocity data is shown in Fig. 12. Again, these data agree well with pitot-static probe data and display good symmetry. The same 4 m/s oscillating pattern is again visible in both cuts through this DGV mean velocity data image (Fig. 11) and as a series of bands near the center of the jet in Fig. 12. Similar DGV jet data have been presented by Naylor at $x/D = 2$, 4, and 6 (Ref. 29). The ability of the present DGV system to respond to the flow turbulence has been investigated by comparing the measurement rms at each pixel location with hot-wire data, and, as expected, the DGV rms levels do not correspond to flow turbulence levels.[29] Clearly, using a continuous wave argon ion laser and unshuttered CCD cameras, as in the present experiments, cannot record flow turbulence. Instead, it would be necessary to utilize a pulsed Nd:YAG laser.

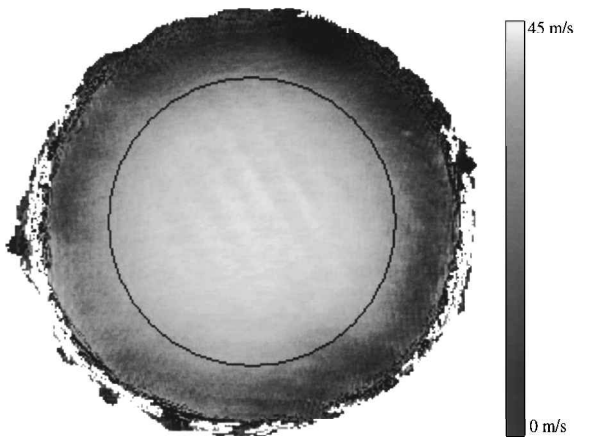

Fig. 12 DGV averaged velocity image of turbulent jet flow, 1 diameter from exit (component 2).

Discussion of Accuracy

For the present DGV mean velocity data in the fully developed turbulent pipe flow and axisymmetric jet flow, key error sources that have been quantified include the following: 1) Noise clearly visible in individual velocity images[4] due to the 8-bit camera resolution has been found to be on the order of ±1 m/s; this is consistent with the observed signal rms errors in the rotating wheel results.[29] 2) The iodine cell calibrations have been found to repeat from day to day to an accuracy of ±1.4 m/s, over a velocity range of 40–60 m/s. 3) Random variations of the side arm temperatures of the reference and measurement iodine cells (rms =0.1°C) have been found to result in rms Doppler shift frequency errors of 1.75 MHz for one cell, corresponding to mean velocity offset errors of between 2 and 10 m/s at 20 : 1 odds (two sigma). 4) Inaccuracies in the flat-field (white card) correction images result in observed measurement variations with a total range of about 4 m/s. 5) The zero velocity tab used to correct for the observed zero velocity offset also has an error with a total range of about 4 m/s.

The first three of these error sources are believed to be random in nature, and independent of one another, and to yield an overall uncertainty of ±2.6–10.1 m/s at 20 : 1 odds when combined as the square root of the sum of the squares. Also, for the present flow apparatus, the blower has been found to reset to an accuracy of ±1 m/s. This results in a total uncertainty estimate due to errors in calibration, truncation errors in the cameras and frame grabber, and iodine cell stem temperature variations of no better than ±5 m/s at a 95% confidence level (20 : 1 odds). This overall error estimate is dominated by the velocity offset error due to side arm temperature variations. The errors due to the flat-field correction image and the zero velocity tab are observed to be on the same order (a total range of about 4 m/s). It is believed that laser speckle noise contributes significantly to both of these error sources. For comparison purposes, the two-component PDV system of Kuhlman et al.[3] gave overall velocity range accuracies of ±1 m/s with an rms noise of ±0.2–0.4 m/s for the rotating wheel, over the same velocity range.[3] However, mean velocity offset errors for the point system were comparable to those of the present DGV system. It is expected that this offset error can be largely eliminated through use of vapor-limited iodine cells in the future.[20–23]

Conclusions

The development of a two-component DGV, along with the corresponding image acquisition and data reduction software, has been described. This DGV system has been patterned after similar systems developed at NASA Langley Research Center in an effort to document accuracies that are attainable with such DGV systems. Results from this system have been presented for the velocity distribution of a rotating wheel, full developed turbulent pipe flow, and axisymmetric jet flow. For the configuration used, the DGV images of rotating wheel velocity data display the expected horizontal bands of constant horizontal wheel velocity. The rms deviation of the DGV wheel velocity data from a linear velocity variation in the Y image

direction was ±1.1 m/s for a single DGV component, corresponding to ±2% of the 59 m/s velocity range. Observed errors in the total measured variation in horizontal velocity across the vertical Y extent of the wheel ranged from 1 to 2 m/s (2 to 4%). Much of this error was due to inaccuracies in the cell calibrations. DGV results for the mean velocity distributions in fully developed turbulent pipe flow and axisymmetric jet flow agreed well with pitot-static probe measurements. The dominant error source for the present DGV system of a randomly varying mean velocity offset has been identified as the result of variations in the side arm temperatures of the reference and measurement iodine cells, with an rms of 0.1°C. These temperature variations yield a predicted mean velocity error of from 2 to 10 m/s, depending on geometry; this is consistent with the observed velocity offset error of 4–5 m/s. The present DGV system is incapable of making accurate rms fluctuation measurements; a pulsed laser would be necessary to resolve fluctuations with timescales smaller than on the order of 1/30th of a second.

Acknowledgments

The present work has been supported under Air Force Office of Scientific Research/DEPSCoR Grants F49620-94-1-0434 and F49620-98-1-0068, James M. McMichael and Mark Glauser, Technical Monitors, as well as NASA Langley Research Center Grant NAG-1-1892, James F. Meyers, Technical Monitor. The authors are grateful for the technical assistance of Jim Meyers, Joe Lee, Rich Schwartz, Angelo Cavone, and Gary Fleming at NASA Langley Research Center, Bob McKenzie and Mike Reinath at NASA Ames Research Center, and Tom Beutner at U.S. Air Force Research Laboratory and to the reviewers for helping to clarify the effects of iodine cell temperature variations on system accuracy.

References

[1]McKenzie, R. L., "Planar Doppler Velocimetry Performance in Low-Speed Flows," AIAA Paper 97-0498, Jan. 1997.

[2]Smith, M. W., and Northam, G. B., "Application of Absorption Filter-Planar Doppler Velocimetry to Sonic and Supersonic Jets," *AIAA Journal*, Vol. 34, No. 3, 1996, pp. 434–441; also AIAA Paper 95-0299, Jan. 1995.

[3]Kuhlman, J. M., Naylor, S., James, K., and Ramanath, S., "Accuracy Study of a Two-Component Point Doppler Velocimeter (PDV)," AIAA Paper 97-1916, June–July 1997.

[4]Naylor, S., and Kuhlman, J., "Accuracy Studies of a Two-Component Doppler Global Velocimeter (DGV)," AIAA Paper 98-0508, Jan. 1998.

[5]Adrian, R. J., and Yao, C. S., "Development of Pulsed Laser Velocimetry for Measurement of Turbulent Flow," *Proceedings of the Eighth Biennial Symposium on Turbulence*, Univ. of Missouri, Rolla, MO, 1983, pp. 170–186.

[6]Dahm, W. J. A., "Scalar Imaging Velocimetry Studies of Turbulent Flow Structure and Dynamics," *Proceedings, AFOSR/ONR Grantee and Contractors Meeting on Turbulence Research*, 1992, pp. 73–76.

[7]Miles, R. B., "RELIEF Measurements of Turbulence," *Proceedings, AFOSR/ONR Grantee and Contractors Meeting on Turbulence Research*, 1992, pp. 62–64.

[8]Komine, H., Brosnan, S. J., Litton, A. B., and Stappaerts, E. A., "Real-Time Doppler Global Velocimetry," AIAA Paper 91-0337, Jan. 1991.

[9]Meyers, J. F., Lee, J. W., and Cavone, A. A., "Signal Processing Schemes for Doppler Global Velocimetry," *IEEE 14th International Congress on Instrumentation in Aerospace Simulation Facilities*, Inst. of Electrical and Electronics Engineers, 1991.

[10]Meyers, J. F., and Komine, H., "Doppler Global Velocimetry: A New Way to Look at Velocity," *ASME 4th International Conference on Laser Anemometry, Advances and Applications*, Vol. 1, American Society of Mechanical Engineers, New York, 1991, pp. 289–296.

[11]Miles, R. B., Lempert, W. R., and Forkey, J., "Instantaneous Velocity Fields and Background Suppression by Filtered Rayleigh Scattering," AIAA Paper 91-0357, Jan. 1991.

[12]Forkey, J. N., Finklestein, N. D., Lempert, W. R., and Miles, R. B., "Control of Experimental Uncertainties in Filtered Rayleigh Scattering Measurements," *AIAA Journal*, Vol. 34, No. 3, 1996, pp. 442–448; also AIAA Paper 95-0298, Jan. 1995.

[13]Hoffenberg, R., and Sullivan, J. P., "Filtered Particle Scattering: Laser Velocimetry Using an Iodine Filter," *ASME Fluids Engineering Division Summer Meeting, Fluid Measurement and Instrumentation Forum*, Vol. 161, American Society of Mechanical Engineers, New York, 1993.

[14]Morrison, G. L., Gaharan, C. A., and DeOtte, R. E., Jr., "Doppler Global Velocimetry: Problems and Pitfalls," *Symposium on Laser Anemometry: Advances and Applications*, FED Vol. 191, American Society of Mechanical Engineers, Fairfield, NJ, 1994, pp. 1–8.

[15]Roehle, I., and Schodl, R., "Evaluation of the Accuracy of the Doppler Global Technique," *Seminar on Optical Methods and Data Processing in Heat and Fluid Flow*, Inst. of Mechanical Engineers, Paper C485/046, 1994.

[16]McKenzie, R. L., "Measurement Capabilities of Planar Doppler Velocimetry Using Pulsed Lasers," *Applied Optics*, Vol. 35, No. 6, 1996, pp. 948–964; also AIAA Paper 95-0297, Jan. 1995.

[17]Smith, M. W., "Application of a Planar Doppler Velocimetry System to a High Reynolds Number Compressible Jet," AIAA Paper 98-0428, Jan. 1998.

[18]Irani, E., "Application and Evaluation of the Doppler Global Velocimetry Method on an Axi-Symmetric Jet," Ph.D. Dissertation, Aerospace Engineering Dept., Wichita State Univ. Wichita, KS, May 1995.

[19]Irani, E., and Miller, L. S., "Evaluation of a Basic Doppler Global Velocimetry System," Society of Automotive Engineers, Paper 951427, May 1995.

[20]Elliott, G. S., Samimy, M., and Arnette, S. A., "Details of a Molecular Filter-Based Velocimetry Technique," AIAA Paper 94-0490, Jan. 1994.

[21]Elliott, G. S., Mosedale, A., Gruber, M. R., Nejad, A. S., and Carter, C. D., "The Study of a Transverse Jet in a Supersonic Cross-Flow Using Molecular Filtered Based Diagnostics," AIAA Paper 97-2999, July 1997.

[22]Clancy, P. S., Samimy, M., and Erskine, W. R., "Planar Doppler Velocimetry: Three-Component Velocimetry in Supersonic Jets," *AIAA Journal*, Vol. 37, No. 6, 1999, pp. 700–707; also AIAA Paper 98-0506, Jan. 1998.

[23]Mosedale, A., Elliott, G. S., Carter, C. D., and Beutner, T. J., "On the Use of Planar Doppler Velocimetry," AIAA Paper 98-2809, June 1998.

[24]Reinath, M. S., "Doppler Global Velocimeter Development for the Large Wind Tunnels at Ames Research Center," NASA TM-112210, Sept. 1997.

[25]Beutner, T. J., and Baust, H. D., "Recent Developments in Doppler Global Velocimetry," AGARD Fluid Dynamics Panel 81st Meeting/Symposium on Advanced Aerodynamic Measurement Technology, Paper 8, Sept. 1997.

[26]Beutner, T. J., Elliott, G., Mosedale, A., and Carter, C., "Doppler Global Velocimetry Applications in Large Scale Facilities," AIAA Paper 99-2608, June 1998.

[27]Ainsworth, R. W., and Thorpe, S. J., "The Development of a Doppler Global Velocimeter for Transonic Turbine Applications," American Society of Automotive Engineers, Paper 94-GT-146, June 1994.

[28]Meyers, J. F., Lee, J. W., Fletcher, M. T., and South, B. W., "Hardening Doppler Global Velocimetry Systems for Large Wind Tunnel Applications," AIAA Paper 98-2606, June 1998.

[29]Naylor, S. M., "Development and Accuracy Determination of a Two-Component Doppler Global Velocimeter (DGV)," Ph.D. Dissertation, Mechanical and Aerospace Engineering Dept., West Virginia Univ., Morgantown, WV, 1998.

[30]Ramanath, S., "Development of a Point Doppler Global Velocimeter (DGV)," M.S. Thesis, Mechanical and Aerospace Engineering Dept., West Virginia Univ., Morgantown, WV, 1997.

[31]James, K., "Determination of the Accuracy of a Two-Component Point Doppler Velocimetry System," M.S. Thesis, Mechanical and Aerospace Engineering Dept., West Virginia Univ., Morgantown, WV, 1997.

[32]Meyers, J. F., "Doppler Global Velocimetry, The Next Generation?," AIAA Paper 92-3897, July 1992.

[33]Meyers, J. F., "Evolution of Doppler Global Velocimetry Data Processing," 8th International Symposium on Applications of Laser Techniques to Fluid Mechanics, Paper 11.1, July 1996.

[34]Wolberg, G., *Digital Image Warping*, IEEE Computer Society Press, Los Alamitos, CA, 1990, Chap. 3, pp. 57–61.

R. P. Lucht
Associate Editor